

# Sign reversal of Magnetoresistivity in massive nodal-line semimetals due to Lifshitz transition of Fermi surface

Min-Xue Yang,<sup>1</sup> Hao Geng,<sup>1,2</sup> Wei Luo,<sup>1,3</sup> Li Sheng,<sup>1,2</sup> Wei Chen,<sup>1,2,\*</sup> and D. Y. Xing<sup>1,2</sup>

<sup>1</sup>*National Laboratory of Solid State Microstructures and department of Physics, Nanjing University, Nanjing, 210093, China*

<sup>2</sup>*Collaborative Innovation Center of Advanced Microstructures, Nanjing University, Nanjing 210093, China*

<sup>3</sup>*School of Science, Jiangxi University of Science and Technology, Ganzhou 341000, China*

Topological nodal-line semimetals offer an interesting research platform to explore novel phenomena associated with its torus-shaped Fermi surface. Here, we study magnetotransport in the massive nodal-line semimetal with spin-orbit coupling and finite Berry curvature distribution which exists in many candidates. The magnetic field leads to a deformation of the Fermi torus through its coupling to the orbital magnetic moment, which turns out to be the main scenario of the magnetoresistivity (MR) induced by the Berry curvature effect. We show that a small deformation of the Fermi surface yields a positive  $MR \propto B^2$ , different from the negative MR by pure Berry curvature effect in other topological systems. As the magnetic field increases to a critical value, a topological Lifshitz transition of the Fermi surface can be induced, and the MR inverts its sign at the same time. The temperature dependence of the MR is investigated, which shows a totally different behavior before and after the Lifshitz transition. Our work uncovers a novel scenario of the MR induced solely by the deformation of the Fermi surface and establishes a relation between the Fermi surface topology and the sign of the MR.

## I. INTRODUCTION

In a solid electronic system, the thermal and transport properties are mainly determined by the electron distribution near the Fermi surface [1]. Therefore, the change of Fermi surface by applying pressure, doping or external field may lead to considerable variation of the electronic properties such as the specific heat and conductivity. Interestingly, apart from continuous deformations, the Fermi surface can also undergo abrupt changes in its topology, so-called topological Lifshitz transition [2]. At such a critical point, anomalies in the thermal and kinetic quantities may appear [2, 3], which may even induce phase transition [4–10].

Besides the topology of the Fermi surface geometry, the electronic band structures can also have nontrivial topology encoded in the Bloch wave functions [11]. In the past two decades, the study on such band topology has opened the exciting research field of topological matters, which includes topological insulators, superconductors, and semimetals [12–14]. The effects of the nontrivial band topology are manifested mainly in two aspects: the existence of exotic surface states on the boundaries of the sample and the modification of the dynamics of the bulk electrons. The latter can give rise to a variety of interesting transport phenomena such as anomalous Hall effect [15], negative longitudinal magnetoresistivity (MR) owing to the chiral anomaly [14, 16–18], and most recently, the nonlinear Hall effect induced by the Berry curvature dipole [19–22].

Given that the deformation of the Fermi surface and nontrivial band topology may appear simultaneously, it is interesting to explore possible novel effects caused by the

interplay between them. In particular, in a topological material with non-vanishing Berry curvature, the interaction between the band topology and the Fermi surface deformation can be achieved by simply applying an external magnetic field. The Berry curvature results in a nonzero orbit magnetic moment (OMM) of the electron [11, 23], of which a coupling with the magnetic field modifies the electronic dispersion and accordingly the shape of the Fermi surface. The benefit of this scenario is that the relevant physical effects can be visibly revealed by the MR measurement. For example, it was shown recently that the coupling of the OMM to the magnetic field in the Weyl semimetal induces a deformation of the Fermi surface from a sphere to an egg shape [24]. As a result, the negative MR due to the chiral anomaly can even have the opposite sign as the inter-node scattering is taken into account simultaneously [24]. Besides the smooth deformation of the Fermi surface, topological Lifshitz transition of the Fermi surface is studied as well in various topological materials [25–30], which is driven by different methods such as the temperature. An interesting question that arises is whether both the smooth deformation and the abrupt Lifshitz transition of the Fermi surface can be implemented by imposing a magnetic field, such that the underlying physics can be manifested under the same framework of MR measurements. Apparently, systems with a Fermi sphere of zero genus is hard to achieve this purpose.

In this work, we study the topological Lifshitz transition of a torus-shaped Fermi surface with genus one in a doped massive nodal-line semimetal [cf. Fig. 1(a)] driven by a magnetic field and predict the corresponding transport signatures. Without a gap opening, the nodal-line semimetals are characterized by the linear band crossing along open lines or closed loops which have been confirmed in a variety of candidates [31–57] and may exhibit interesting transport properties [58–60]. The topologi-

---

\* Corresponding author: pchenweis@gmail.com

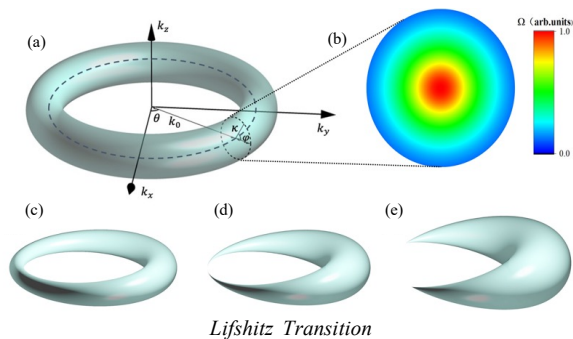


FIG. 1. (a) Schematic diagram of the torus-shaped Fermi surface in nodal-line semimetal, with the major radius  $k_0$ , minor radius  $\kappa$ , toroidal angle  $\theta$ , and poloidal angle  $\varphi$ . (b) Finite distribution of Berry curvature in the poloidal cross section. (c)-(e) Fermi surface deformation induced by the magnetic field, with (c) a slight deformation, (d) critical point of topological Lifshitz transition and (e) Fermi surface with genus one.

cal property of the bands is encoded in the  $\pi$  Berry flux carried by the nodal line, while the Berry curvature vanishes elsewhere in the Brillouin zone. As a result, the OMM and its coupling to the magnetic field are absent without spin-orbit coupling. However, sizable spin-orbit coupling generally exists in many candidates of the nodal-line semimetals, which may give rise to a gap  $\Delta$  of order 10-100 meV in the energy spectrum [61, 62]. In these materials, the  $\pi$  Berry flux spreads into a finite-region distribution of the Berry curvature in the momentum space; see Fig. 1(b). As the sample is slightly doped, a deformation of the Fermi torus can be achieved by coupling the OMM with the external magnetic field  $B$ ; see Figs. 1(c)-1(e).

Here, we study the magnetotransport in the massive nodal-line semimetals in the diffusive limit by using the semiclassical Boltzmann formalism and taking into account the Berry curvature effect. We show that the OMM induced deformation of the Fermi surface is the key scenario for the MR, in contrast to the negative MR in other topological materials by pure Berry curvature effect without OMM [18, 63]. Specifically, it is found that a slight deformation of the Fermi torus results in a positive MR  $\propto B^2\Delta^2$ ; Remarkably, as  $B$  increases to a critical value, the topological Lifshitz transition occurs for the Fermi surface [cf. Fig. 1(d)], which is proved to coincide with a sign reversal of the MR. Our results provide a new perspective to understand the MR in nodal-line semimetals and establish a fascinating relationship between the sign of MR and the Fermi surface topology.

The rest of this paper is organized as follows. In Sec. II, we calculate the OMM in the massive nodal-line semimetal and its coupling to the magnetic field; In Sec. III, we derive the general conductance formula using the semiclassical Boltzmann equation. In Sec. IV, we study the magnetic transport properties and their physical origins both analytically and numerically. In Sec.

V, we give a discussion on the different manifestation of our scenario from others. In Sec. VI, we draw our main conclusion.

## II. OMM IN MASSIVE NODAL-LINE SEMIMETALS

We start with a minimal model of the nodal-line semimetal with two bands crossing along a single nodal loop as [31]

$$H_0 = \hbar\lambda(k_x^2 + k_y^2 - k_0^2)\tau_x + \hbar v k_z \tau_y, \quad (1)$$

where  $\tau_{x,y}$  are the Pauli matrices acting on the orbital degree of freedom. The eigenvalues of the Hamiltonian  $\epsilon_{\mathbf{k}} = \pm\sqrt{\hbar^2\lambda^2(k_x^2 + k_y^2 - k_0^2)^2 + \hbar^2v^2k_z^2}$  defines a band-degeneracy line  $k_x^2 + k_y^2 = k_0^2$ , that is a nodal loop with a radius  $k_0$  in the reciprocal space. The energy scale near the band crossing is of most interest, where the Hamiltonian (1) can be linearized and parameterized to [59]

$$H = \hbar v_0 \kappa (\cos \varphi \tau_x + \sin \varphi \tau_y), \quad (2)$$

through the substitution  $k_x = (k_0 + \kappa \cos \varphi) \cos \theta$ ,  $k_y = (k_0 + \kappa \cos \varphi) \sin \theta$ ,  $k_z = \kappa \sin \varphi / \alpha$  with  $v_0 = 2\lambda k_0$  and  $\alpha = v/v_0$  the ratio between the velocity along the  $z$  direction and that in the  $x$ - $y$  plane. The parameters  $\kappa, \theta, \varphi$  are the coordinates defined on the torus as shown in Fig. 1(a).

In the presence of spin-orbit coupling, a mass term should be added as [61]

$$\mathcal{H} = H + \Delta \tau_z \sigma_z, \quad (3)$$

with its sign depending on that of the spin  $\sigma_z$ . Accordingly, the energy spectrum becomes  $\epsilon_{\mathbf{k}}^{\pm}(\kappa) = \pm\sqrt{(\hbar v_0 \kappa)^2 + \Delta^2}$ , in which a gap of  $2\Delta$  is induced along the nodal loop. We focus on the regime that the effect due to the Zeeman coupling between the magnetic field and the spin is negligibly small. Then it can be shown that the main results do not rely on the spin or equivalently, the sign of the mass, so that we set  $\sigma_z = 1$  in the following.

Without loss of generality, we consider a positive Fermi energy, such that only the electrons in the conduction band contributes to the transport and the wave function is found to be  $|u_{\mathbf{k}}\rangle = (\kappa e^{-i\varphi} / \sqrt{\kappa^2 + \gamma^2}, \gamma / \sqrt{\kappa^2 + \gamma^2})$  with  $\gamma = \sqrt{m^2 + \kappa^2} - m$  and  $m = \Delta / (\hbar v_0)$ . The Berry curvature defined by  $\mathbf{\Omega}_{\mathbf{k}} = i\langle \nabla_{\mathbf{k}} u_{\mathbf{k}} | \times | \nabla_{\mathbf{k}} u_{\mathbf{k}} \rangle$  has only a nonzero value along the toroidal direction in the parametric coordinates as

$$\mathbf{\Omega}_{\mathbf{k}} = -\frac{m}{2(\kappa^2 + m^2)^{\frac{3}{2}}} \hat{e}_{\theta}, \quad (4)$$

which reduces to a Berry flux density as  $m \rightarrow 0$ . The Berry curvature induces a self-rotation of the electron wave packet which gives rise to a finite OMM [11, 23]. In

the present two band system, the OMM is related to the Berry curvature through  $\mathcal{M}_{\mathbf{k}} = \frac{e}{2\hbar} \mathbf{\Omega}_{\mathbf{k}} (\epsilon_{\kappa}^+ - \epsilon_{\kappa}^-)$ , yielding

$$\mathcal{M}_{\mathbf{k}} = -\frac{mev_0}{2(\kappa^2 + m^2)} \hat{e}_\theta, \quad (5)$$

which is also a vector field along the toroidal direction.

One can infer that as an external magnetic field is imposed, only its components in the  $x$ - $y$  plane couple to the OMM. Without loss of generality, we consider a magnetic field  $\mathbf{B} = B\hat{x}$  in the  $x$ -direction, which gives rise to a coupling energy as

$$\delta\epsilon_{\mathbf{k}}(\kappa, \theta) = -\mathcal{M}_{\mathbf{k}} \cdot \mathbf{B} = -(mev_0 B) \sin\theta / [2(\kappa^2 + m^2)]. \quad (6)$$

The whole energy of the conduction band becomes

$$\tilde{\epsilon}_{\mathbf{k}}(\kappa, \theta) = \epsilon_{\mathbf{k}}^+(\kappa) + \delta\epsilon_{\mathbf{k}}(\kappa, \theta), \quad (7)$$

which now depends on the toroidal angle  $\theta$ . A direct result of this anisotropy is a deformation of the Fermi torus, as shown in Figs. 1(c)-1(e). We will demonstrate in the following that such a deformation is the main scenario of the magnetotransport.

### III. SEMICLASSICAL THEORY

In this section, we solve the transport problem in the presence of impurity scattering using the semiclassical Boltzmann formalism. We assume that the magnetic field satisfies  $B \ll \epsilon_F / (v_0^2 e \tau)$  with  $\epsilon_F$  the Fermi energy and  $\tau$  the elastic scattering time, which means that the Landau level spacing  $\hbar v_0^2 e B / \epsilon_F$  near the Fermi energy is much less than the energy uncertainty  $\hbar / \tau$  due to scattering and thus the effects of the Landau quantization can be ignored. The semiclassical equations of motion are given by [11, 64]

$$\dot{\mathbf{r}} = \frac{1}{\hbar} \nabla_{\mathbf{k}} \tilde{\epsilon}_{\mathbf{k}} - \dot{\mathbf{k}} \times \mathbf{\Omega}_{\mathbf{k}}, \quad \dot{\mathbf{k}} = -\frac{e}{\hbar} (\mathbf{E} + \dot{\mathbf{r}} \times \mathbf{B}), \quad (8)$$

where  $\mathbf{r}$  and  $\mathbf{k}$  are the central position and momentum of the wave packet, respectively.  $-e$  is the electron charge, and  $\mathbf{E}$  and  $\mathbf{B}$  are the external electric and magnetic fields. We focus on the linear-response regime ( $\mathbf{E} = 0$ ) and solving Eq. (8) gives an effective velocity as

$$\dot{\mathbf{r}} = [\tilde{\mathbf{v}}_{\mathbf{k}} + (e/\hbar) \mathbf{B} (\tilde{\mathbf{v}}_{\mathbf{k}} \cdot \mathbf{\Omega}_{\mathbf{k}})] / D_{\mathbf{k}}, \quad (9)$$

where  $D_{\mathbf{k}}^{-1}$  is the correction to the density of states [65] with

$$D_{\mathbf{k}} = 1 + \frac{e}{\hbar} \mathbf{B} \cdot \mathbf{\Omega}_{\mathbf{k}}, \quad (10)$$

and  $\tilde{\mathbf{v}}_{\mathbf{k}} = (1/\hbar) \nabla_{\mathbf{k}} \tilde{\epsilon}_{\mathbf{k}}$  yields

$$\tilde{\mathbf{v}}_{\mathbf{k}} = \mathbf{v}_{\mathbf{k}} - \frac{1}{\hbar} \nabla_{\mathbf{k}} (\mathcal{M}_{\mathbf{k}} \cdot \mathbf{B}). \quad (11)$$

One can see that apart from the pure effect of the Berry curvature on the velocity in Eq. (9), the OMM introduces a correction of the velocity as  $\mathbf{v}_{\mathbf{k}} \rightarrow \tilde{\mathbf{v}}_{\mathbf{k}}$ , which is

essential for the MR in the massive nodal-line semimetals. Similarly, we have

$$\dot{\mathbf{k}} = -\frac{e}{\hbar D_{\mathbf{k}}} \left[ \mathbf{E} + \tilde{\mathbf{v}}_{\mathbf{k}} \times \mathbf{B} + \frac{e}{\hbar} (\mathbf{B} \cdot \mathbf{E}) \mathbf{\Omega}_{\mathbf{k}} \right]. \quad (12)$$

The steady Boltzmann equation is interpreted as

$$\dot{\mathbf{k}} \cdot \nabla_{\mathbf{k}} f = -\frac{f - f_0}{\tau}, \quad (13)$$

where a uniform condition and the relaxation time approximation are adopted. The function  $f$  is the distribution function and  $f_0 = 1/[e^{(\tilde{\epsilon}_{\mathbf{k}} - \epsilon_F)/k_B T} + 1]$  is the Fermi-Dirac equilibrium distribution. Substituting Eq. (12) into Eq. (13) and keeping the terms to the first order of  $\mathbf{E}$  on both sides yields

$$f_1 = \frac{e\tau}{D_{\mathbf{k}}} \left[ \mathbf{E} + \frac{e}{\hbar} (\mathbf{E} \cdot \mathbf{B}) \mathbf{\Omega}_{\mathbf{k}} \right] \cdot \tilde{\mathbf{v}}_{\mathbf{k}} \frac{\partial f_0}{\partial \tilde{\epsilon}}. \quad (14)$$

where  $f_1 = f - f_0$  is the first-order deviation of the distribution from the equilibrium. The current density is solved by

$$\mathbf{J} = -e \int \frac{d\mathbf{k}}{(2\pi)^3} f_1 D_{\mathbf{k}} \dot{\mathbf{r}}, \quad (15)$$

and the longitudinal conductivity defined by  $J_\mu = \sigma_\mu E_\mu$  ( $\mu = x, y, z$ ) takes the form of [63]

$$\sigma^\mu = - \int \frac{d^3\mathbf{k}}{(2\pi)^3} \frac{e^2 \tau}{D_{\mathbf{k}}} (\tilde{v}_{\mathbf{k}}^\mu + \frac{e}{\hbar} B^\mu \tilde{\mathbf{v}}_{\mathbf{k}} \cdot \mathbf{\Omega}_{\mathbf{k}})^2 \frac{\partial f_0}{\partial \tilde{\epsilon}} \quad (16)$$

### IV. MANETOTRANSPORT PROPERTIES

First, we note that a magnetic field  $\mathbf{B} = B\hat{z}$  in the  $z$ -direction has no coupling to the OMM, i.e.,  $\mathcal{M}_{\mathbf{k}} \cdot \mathbf{B} = 0$ , which does not result in any deformation of the Fermi torus. Accordingly, we have  $\tilde{\mathbf{v}}_{\mathbf{k}} = \mathbf{v}_{\mathbf{k}}$  and  $\tilde{\mathbf{v}}_{\mathbf{k}} \cdot \mathbf{\Omega}_{\mathbf{k}} = 0$  in Eq. (16), which indicates that no  $\mathbf{B}$ -dependence of the conductivity or MR appears. Hereafter, we consider the external magnetic field applied in the  $x$ -direction, so that a coupling between the OMM and the magnetic field can be achieved. It induces a deformation of the Fermi torus which increases with  $B$  and the gap  $\Delta$  induced by the spin-orbit coupling. Moreover, the conductivity in Eq. (16) depends on  $\mathbf{B}$  in general, indicating a MR induced by the deformation of the Fermi torus.

#### A. Symmetry analysis

Before we go to further details, let us first perform a symmetry analysis on the conductivity  $\sigma(B, m)$ . Note that Eq. (16) is invariant as  $B$  and  $m$  change their signs simultaneously, that is

$$\sigma^\mu(B, m) = \sigma^\mu(-B, -m). \quad (17)$$

Additionally, the nodal-line semimetal possesses the rotation symmetry about the  $z$ -axis, which means that as we invert both  $\mathbf{B}$  and  $\mathbf{E}$  (equivalent to a rotation of the fields by  $\pi$ ), the conductivity remains the same, that is

$$\sigma^\mu(B, m) = \sigma^{-\mu}(-B, m). \quad (18)$$

Finally, the following relation holds,

$$\sigma^\mu(B, m) = \sigma^{-\mu}(B, m), \quad (19)$$

which ensures that there is no spontaneous current flowing as  $\mathbf{E} = 0$ . Combining Eqs. (17), (18) and (19) leads to

$$\begin{aligned} \sigma^\mu(B, m) &= \sigma^\mu(B, -m), \\ \sigma^\mu(B, m) &= \sigma^\mu(-B, m), \end{aligned} \quad (20)$$

which shows that  $\sigma^\mu(B, m)$  is an even function of both  $B$  and  $m$  and confirms that the MR is independent of the sign of the mass as mentioned before. It is convenient to separate the conductivity to two terms as  $\sigma^\mu(B, m) = \sigma_0^\mu + \delta\sigma^\mu(B, m)$ , with  $\sigma_0^\mu$  the Drude conductivity for  $B = 0$  and  $\delta\sigma^\mu(B, m)$  being the magnetoconductivity, which scales as  $\propto B^2 m^2$  to the lowest order of  $B$  and  $m$  according to the symmetry analysis above.

### B. Slight Fermi torus deformation and positive MR

In order to get some analytic results, we first solve the conductivity (16) in the weak field limit  $B \ll \epsilon_F^2/(\hbar v_0^2)$ , i.e., the Landau level spacing is much smaller than the Fermi energy. This condition is equivalent to  $\kappa_F \ell_B \gg 1$ , with  $\kappa_F = \epsilon_F/(\hbar v_0)$  the Fermi wave vector and  $\ell_B = \sqrt{\hbar/(eB)}$  the magnetic length. Moreover, we also assume that  $\kappa_F \gg m$ , such that the spin-orbit coupling can be considered as a perturbation. The zero-temperature conductivity calculated by Eq. (16) is obtained as (see the Appendix A for details)

$$\begin{aligned} \sigma_0^x &= \sigma_0^y = \sigma_0^z/2\alpha^2 = \frac{e^2 k_0 \epsilon_F \tau}{8\pi\alpha\hbar^2}, \\ \delta\sigma^x &= \delta\sigma^y/3 = \delta\sigma^z/4\alpha^2 = -\frac{3\alpha e^4 v_0^6 \hbar^2 k_0 \tau}{32\pi\epsilon_F^5} B^2 m^2, \end{aligned} \quad (21)$$

which is consistent with our symmetry analysis that  $\delta\sigma^\mu \propto B^2 m^2$ . The magnetic conductivities in three directions differ from each other by noting that the deformation of the Fermi torus breaks the rotational symmetry in the  $x$ - $y$  plane.

Here, the coupling between the OMM and the magnetic field and the resultant deformation of the Fermi surface play a decisive role for the magnetoconductivity; The pure Berry curvature effect cannot lead to this result. This is in stark contrast to the situations for the Weyl semimetal [18] and the topological insulator [63], where the finite Berry curvature leads to a negative MR.

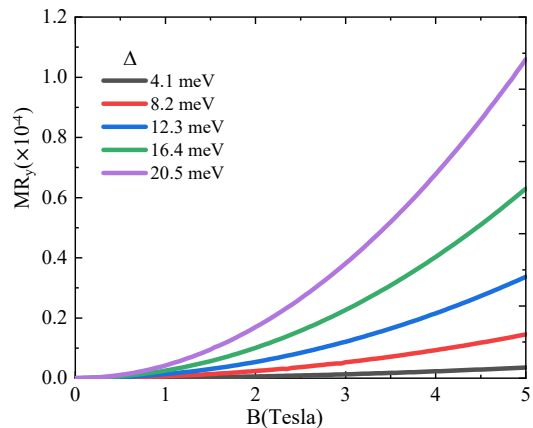


FIG. 2. MR as a function of magnetic field  $B$  for different gap  $\Delta$  in the regime of slight Fermi surface deformation. The relevant parameters are  $\epsilon_F = 41$  meV,  $T = 5$  K,  $k_0 = 10$  nm $^{-1}$ ,  $\tau = 10^{-14}$  s and  $v_0 = 10^5$  m/s.

The results in Eq. (21) indicate a *positive* longitudinal MR in the weak field limit defined by

$$\text{MR}_\mu(B) = \frac{1/\sigma^\mu(B) - 1/\sigma^\mu(0)}{1/\sigma^\mu(0)}. \quad (22)$$

Therefore, the MR ( $\propto B^2 m^2$ ) induced by the Berry curvature through the OMM effect in the massive nodal-line semimetal is opposite in sign to that of the Weyl semimetal (in the absence of inter-node scattering) [18, 24] and the topological insulator [63]. Note that the OMM induced deformation of the Fermi surface also introduces a positive correction to the MR in the Weyl semimetal [24], which is in agreement with our results.

### C. Lifshitz transition and sign reversal of MR

In the previous section, our analytical results show that a slight deformation of the Fermi torus yields a positive MR which exhibits the  $B^2$  dependence of the magnetic field. In this section, we evaluate the conductivity in Eq. (16) numerically for more general cases. First, the numerical results for the limit  $\kappa_F \gg m$  shown in Fig. 2 confirm the  $B^2$  scaling of the positive MR. A stronger deformation of the Fermi torus occurs as either  $\mathbf{B}$  or the ratio  $m/\kappa_F$  increases, which yields a stronger coupling between  $\mathbf{B}$  and the OMM. Interestingly, the MR does not obey a monotonic dependence on  $B$ , which can be seen in Fig. 3(a). The MR first goes up to its maximum and then drops rapidly as  $B$  increases; Dramatically, the MR changes its sign from positive to negative as  $B$  increases further.

The sign reversal of the MR induced by the Berry curvature cannot be found in other topological systems such as Weyl semimetals [18] and topological insulators [63], which indicates a possible new physical scenario of the

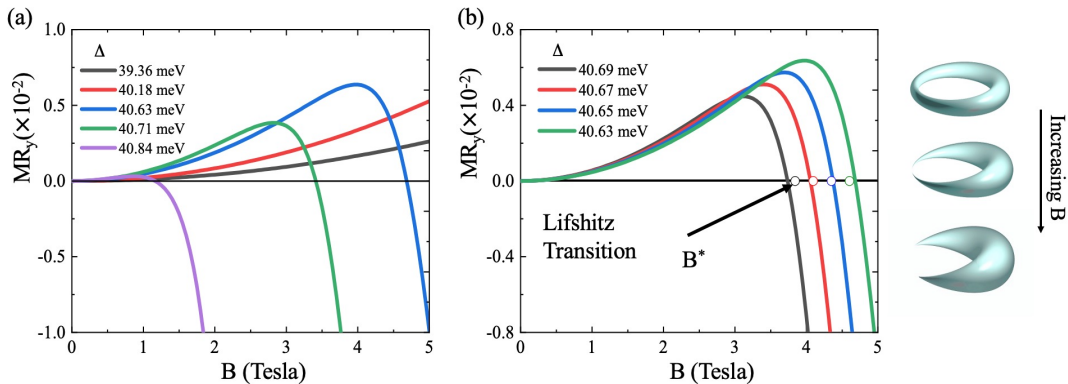


FIG. 3. (a) MR as a function of  $B$  for different gap  $\Delta$  with and without sign reversal. (b) Correspondence between the sign reversal point and the critical field  $B^*$  (open circles) for the Lifshitz phase transition. The right panel of (b) illustrates the Lifshitz transition induced by the magnetic field, which can be compared with the MR results. Other parameters are the same as those in Fig. 2.

MR in the massive nodal-line semimetal. Note that a key difference between the nodal-line semimetal and other topological systems lies in its nontrivial Fermi surface topology. In contrast to a conventional Fermi sphere, the Fermi torus may undergo a topological Lifshitz transition at some critical point from genus one to zero [cf. Fig. 1]. Such abrupt change of the Fermi surface can lead to anomalous physical properties [2–10], which provides a possible explanation for the sign reversal of the MR. In the following, we prove that it is the Lifshitz transition that inverts the sign of the MR.

Next, we focus on the limit  $\kappa_F \ll m$  which generates a thin Fermi torus with the Lifshitz transition taking place with an accessible field strength. We mark the critical field  $B^*$  for the Lifshitz transition points by open circles in Fig. 3(b). One can see a good coincidence between  $B^*$  and the sign reversal points of the MR. The numerical results are obtained by setting the temperature to  $T = 0.25$  K rather than absolute zero (due to the computational capability). We have confirmed the tendency that the match between critical  $B^*$  and the sign reversal points gets better as  $T$  decreases, indicating a strong connection between the sign change of the MR and the topological Lifshitz transition of the Fermi torus.

Moreover, the scenario of topological Lifshitz transition induced sign reversal of the MR can be proved strictly in the limit  $\kappa_F \ll m$ , where the energy can be expressed as  $\epsilon_F \simeq \hbar v_0(m + \eta)$  with the parameter  $\eta \ll m$ . The critical field for the Lifshitz transition can be obtained as  $B^* = 2\hbar m \eta / e$ . By expanding the expression of the conductance in Eq. (16) to the linear order of  $\eta$ , we obtain  $\sigma^\mu(B^*) = \sigma^\mu(0)$ , which means that the Lifshitz transition coincides exactly the sign reversal point of the longitudinal MR in all three directions [see Appendix B for details].

#### D. Finite temperatures

Next, we investigate the effect of finite temperature on the MR in Fig. 4. We choose the magnetic field  $B$  and the gap  $\Delta$  to be fixed so that the deformation of the Fermi surface is determined by the energy. As  $\epsilon_F > 20.5$  meV, the critical value for the Lifshitz transition defined at zero temperature, the genus of the Fermi surface is one, corresponding to a slight deformation; see the inset of Fig. 4(a). In this regime, the positive MR first increases with temperature and then undergoes a rapid decrease to zero, exhibiting a non-monotonic behavior. For  $\epsilon_F < 20.5$  meV, Lifshitz transition occurs and the genus of the Fermi surface becomes zero; see the inset of Fig. 4(b). Correspondingly, the MR is negative and its magnitude decreases monotonically to zero as the temperature rises; see Fig. 4(b).

One can see that in the two regimes with genus equal to one or zero, the temperature cannot invert the sign of the MR. This indicates that the sign of the MR provides a robust signature of the topology of the Fermi surface against finite temperature effect. Moreover, the different temperature dependence of the MR in the two regimes can serve as an additional manifestation for the identification of the Fermi surface topology. For the low temperature, a smaller magnitude of the MR corresponds to a larger Fermi energy in Figs. 4(a) and 4(b). This stems from that for a higher energy, the coupling between the OMM and the magnetic field becomes weaker, which has the same effect as the reduction of the gap  $\Delta$  as shown in Fig. 2. For sufficiently high temperature  $k_B T \sim \epsilon_F - \Delta$ , the Fermi surface is no longer well defined so that the MR induced by its deformation quenches. Finally, at the critical point of Lifshitz transition  $\epsilon_F \simeq 20.5$  meV, MR equals zero for both  $T = 0$  and  $T \gg (\epsilon_F - \Delta)/k_B$  and possesses a negative value in between.



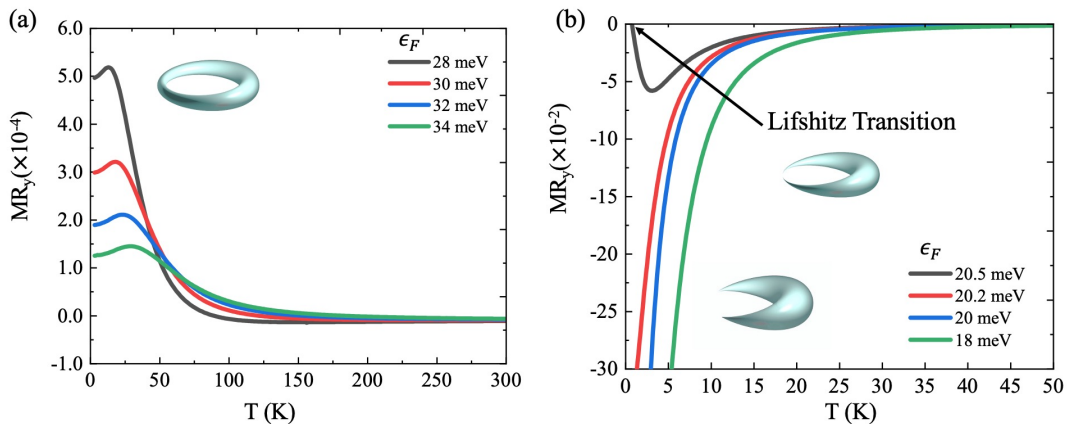


FIG. 4. Temperature dependence of MR for different Fermi energies  $\epsilon_F$  (a) without and (b) with Lifshitz transition illustrated by the inset. The parameters are  $\Delta = 20$  meV,  $B = 3$  T and the others are the same as those in Fig. 2.

## V. DISCUSSIONS

It is important to compare our results to other scenarios of the MR and their manifestation in the nodal-line semimetals. The existing transport experiments on the nodal-line semimetals have reported a variety of transport properties [55, 56, 66–71], such as large positive MR [55, 56, 66–69] or cusp-like behavior of MR in low magnetic field [69, 70]. Different mechanisms have been adopted to explain these results, such as the electron-hole compensation [55, 66, 68] and weak localization and anti-localization [67, 69, 70]. The former results in a positive MR with a  $B^2$  dependence, no much different from that in a conventional metal [1]; The latter may lead to either weak localization or anti-localization with  $\sqrt{B}$  or  $\ln B$  scaling which is determined by the type of the impurity the resultant diffusion dimensionality [62].

The OMM induced MR predicted in our work can be discriminated from both mechanisms above. First, the MR exhibits a non-monotonic  $B$  dependence for a strong deformation of the Fermi torus which can even invert its sign as  $B$  approaches  $B^*$  [cf. Fig. 3]. Such a phenomenon has not been discovered previously, which can be explained neither by the electron-hole compensation nor the weak (anti-)localization effect. It can serve as a unique transport property of the topological Lifshitz transition induced by the coupling between OMM and magnetic field. Second, the MR is positive and proportional to  $B^2$  for the slight deformation of the Fermi torus when  $B \ll B^*$  [cf. Fig. 2], which differs in sign from the weak localization and in scaling law from the weak anti-localization scenario [67, 69, 70]. The mechanism of electron-hole compensation results in the same sign and scaling, but it gives an MR whose magnitude is several orders larger than that in our results [55, 66, 68]. Third, the distinctive temperature dependence of the MR in the two regimes with genus one and zero [cf. Fig. 4] further helps to discriminate the current mechanism from others.

## VI. CONCLUSIONS

To conclude, we predict a novel mechanism for the magnetotransport in nodal-line semimetals which stems from the Fermi surface deformation induced by the coupling between the OMM and magnetic field. Specifically, a small deformation results in a positive MR with a quadratic dependence of  $B$ ; Most interestingly, the strong distortion causes the topological Lifshitz transition of the Fermi torus that is in coincidence with a sign reversal of the MR. The key ingredient of our mechanism is the spin-orbit coupling induced mass term which exists in many nodal-line semimetal candidates [61, 62]. Large spin-orbit coupling and low Fermi energy are favorable for the realization of strong Fermi surface deformation and Lifshitz transition. Our work uncovers a novel scenario of the MR induced solely by the Fermi surface deformation, which also opens an avenue for studying topological Lifshitz transition by magnetotransport.

## ACKNOWLEDGMENTS

We thank Jing Luo for assistance on the figures. This work was supported by the National Natural Science Foundation of China under Grant No. 12074172 (W.C.), No. 11674160 and No. 11974168 (L.S.), the startup grant at Nanjing University (W.C.), the State Key Program for Basic Researches of China under Grants No. 2017YFA0303203 (D.Y.X.) and the Excellent Programme at Nanjing University.

### Appendix A: Magnetoconductivity with slight deformation of the Fermi torus

Here, we provide a detailed derivation of the magnetoconductivity as the deformation of the Fermi torus is

weak. We first solve the conductivity with  $\alpha = 1$  and then generalize the results to  $\alpha \neq 1$ . The expression of the conductivity (16) contains various terms. The velocity components in the cartesian coordinates are

$$\begin{aligned}\tilde{v}_x &= -\tilde{v}_\theta \sin \theta + \tilde{v}_\kappa \cos \theta \cos \varphi, \\ \tilde{v}_y &= \tilde{v}_\theta \cos \theta + \tilde{v}_\kappa \sin \theta \cos \varphi, \\ \tilde{v}_z &= \tilde{v}_\kappa \sin \varphi,\end{aligned}\quad (\text{A1})$$

with

$$\begin{aligned}\tilde{v}_k &= v_0 \left( \frac{\kappa}{\sqrt{\kappa^2 + m^2}} + \frac{B\epsilon\kappa m \sin \theta}{\hbar(\kappa^2 + m^2)^2} \right) \\ \tilde{v}_\theta &= -\frac{Bemv_0 \cos \theta}{2\hbar(\kappa^2 + m^2)(k_0 + \kappa \cos \varphi)} \\ \tilde{v}_\varphi &= 0\end{aligned}\quad (\text{A2})$$

We focus on the weak field limit  $B \ll \epsilon_F^2/(\hbar v_0^2)$  and  $m/\kappa_F \ll 1$  so that  $\epsilon_{\mathbf{k}} \simeq \hbar v_0 \kappa$  and

$$\begin{aligned}\tilde{v}_\kappa &\simeq v_0 \left( 1 + \frac{m \sin \theta}{\ell_B^2 \kappa^3} \right), \\ \tilde{v}_\theta &\simeq -v_0 \frac{m \cos \theta}{2\ell_B^2 \kappa^2 k_0}, \\ \tilde{v}_\varphi &= 0.\end{aligned}\quad (\text{A3})$$

The correction to the density of states reduces to

$$\frac{1}{D_{\mathbf{k}}} \simeq 1 - \frac{m \sin \theta}{2\ell_B^2 \kappa^3}.\quad (\text{A4})$$

Note that the distribution function  $f_0$  in Eq. (16) is a function of  $\tilde{\epsilon}_{\mathbf{k}}$  instead of  $\epsilon_{\mathbf{k}}$ . In the aforementioned limit, we have

$$\delta\epsilon_{\mathbf{k}} \simeq -\hbar^3 m v_0^3 \sin \theta / (2\ell_B^2 \epsilon^2),\quad (\text{A5})$$

and accordingly

$$\begin{aligned}\frac{\partial f_0}{\partial \tilde{\epsilon}} &= \frac{\partial f_0(\epsilon + \delta\epsilon)}{\partial \epsilon} \frac{\partial \epsilon}{\partial \tilde{\epsilon}} \\ &\simeq \frac{\partial [f_0(\epsilon) + f_0'(\epsilon)\delta\epsilon]}{\partial \epsilon} \left( 1 - \frac{\partial \delta\epsilon}{\partial \epsilon} \right) \\ &= (f_0' + \delta\epsilon' f_0' + \delta\epsilon f_0'') (1 - \delta\epsilon'),\end{aligned}\quad (\text{A6})$$

which further reduces to

$$\frac{\partial f_0(\tilde{\epsilon})}{\partial \tilde{\epsilon}} \simeq \frac{\partial f_0(\epsilon)}{\partial \epsilon} + \delta\epsilon \frac{\partial^2 f_0(\epsilon)}{\partial \epsilon^2},\quad (\text{A7})$$

by keeping the terms to the linear order of  $\delta\epsilon$ . By inserting all these simplified terms into the integration in Eq. (16) and transferring the integral variables to  $(\kappa, \theta, \varphi)$ , the conductivity at zero temperature can be obtained as  $\sigma^\mu = \sigma_0^\mu + \delta\sigma^\mu$  with

$$\begin{aligned}\sigma_0^x &= \sigma_0^y = \sigma_0^z / 2 = \frac{e^2 k_0 \epsilon_F \tau}{8\pi \hbar^2}, \\ \delta\sigma^x &= \delta\sigma^y / 3 = \delta\sigma^z / 4 = -\frac{3e^4 v_0^6 \hbar^2 k_0 \tau}{32\pi \epsilon_F^5} B^2 m^2,\end{aligned}\quad (\text{A8})$$

in which the condition  $k_0 \gg \kappa_F$  is adopted.

The results for  $\alpha \neq 1$  can be obtained straightforwardly by the substitutions  $k_z \rightarrow \alpha k_z$  and accordingly,  $\Omega_z(k_z) \rightarrow \Omega_z(\alpha k_z)$ ,  $\Omega_{x,y}(k_z) \rightarrow \alpha \Omega_{x,y}(\alpha k_z)$ ,  $\mathcal{M}_z(k_z) \rightarrow \mathcal{M}_z(\alpha k_z)$ ,  $\mathcal{M}_{x,y}(k_z) \rightarrow \alpha \mathcal{M}_{x,y}(\alpha k_z)$ , which yields

$$\begin{aligned}\sigma_0^x &= \sigma_0^y = \sigma_0^z / 2\alpha^2 = \frac{e^2 k_0 \epsilon_F \tau}{8\pi \alpha \hbar^2}, \\ \delta\sigma^x &= \delta\sigma^y / 3 = \delta\sigma^z / 4\alpha^2 = -\frac{3\alpha e^4 v_0^6 \hbar^2 k_0 \tau}{32\pi \epsilon_F^5} B^2 m^2,\end{aligned}\quad (\text{A9})$$

which is the Eq. (21) in the main text.

## Appendix B: Proof of the correspondence between the Lifshitz transition and sign reversal of MR

In this section, we prove the coincidence between the Lifshitz phase transition of the Fermi torus and the sign reversal point of the MR in the limit  $\kappa_F \ll m$ . Without loss of generality, we focus on the longitudinal conductivity in the  $y$  direction and express Eq. (16) in the parametric coordinates as

$$\begin{aligned}\sigma^y(B) &= -\int \frac{e^2 \tau}{(2\pi)^3} \frac{\kappa(k_0 + \kappa \cos \varphi)}{D_{\mathbf{k}}} \\ &\quad \times (\tilde{v}_\theta \cos \theta + \tilde{v}_\kappa \sin \theta \cos \varphi)^2 \frac{\partial f_0}{\partial \tilde{\epsilon}} d\kappa d\theta d\varphi,\end{aligned}\quad (\text{B1})$$

where  $\tilde{v}_\theta$  and  $\tilde{v}_\kappa$  take the general form in Eq. (A2). Note that  $\tilde{v}_\theta \ll \tilde{v}_\kappa$  generally holds, we can neglect  $\tilde{v}_\theta \cos \theta$  term in the parentheses. The Lifshitz transition can be induced by an accessible magnetic field in the limit  $\kappa_F \ll m$ , in which the energy can be expressed as  $\epsilon_F = \hbar v_0(m + \eta)$  with  $\eta \ll m$ . The critical field  $B^*$  for the Lifshitz transition is defined by

$$\tilde{\epsilon}(\kappa = 0, \theta = -\pi/2, B = B^*) = \epsilon_F,\quad (\text{B2})$$

which gives the critical magnetic field

$$B^* = 2\hbar m \eta / e\quad (\text{B3})$$

by neglecting  $(\kappa/m)^2$  terms.

Next we evaluate the integration in Eq. (B1) at the critical point  $B^*$  in which the relevant terms can be simplified to

$$\begin{aligned}\frac{\partial f_0}{\partial \tilde{\epsilon}} &\simeq \delta[\hbar v_0 \kappa^2 / (2m) - \hbar v_0 \eta (\sin \theta + 1)], \\ \frac{1}{D_{\mathbf{k}}} &\simeq \left( 1 - \frac{\eta}{m} \sin \theta \right), \\ \tilde{v}_\kappa &= v_0 \frac{\kappa}{\sqrt{m^2 + \kappa^2}} \left( 1 + \frac{2\eta \sin \theta}{m} \right)\end{aligned}\quad (\text{B4})$$

in the limit  $\kappa \ll m$ . By performing the integration by keeping the term  $\eta/m$  to its first order we arrive at

$$\sigma^y(B^*) = \sigma_0^y,\quad (\text{B5})$$

which means that at the critical field for the topological Lifshitz transition, the magnetoconductivity and thus the MR is zero, corresponding to the sign reversal point of

the MR [cf. Fig. 3(b) in the main text]. The same conclusion of the MR in the  $x$  and  $z$  directions can also be proved in a similar way.

- 
- [1] C. Kittel and P. McEuen, *Introduction to solid state physics*, Vol. 8 (Wiley New York, 1996).
- [2] I. Lifshitz *et al.*, Sov. Phys. JETP **11**, 1130 (1960).
- [3] T. Nishimura, H. Sakai, H. Mori, K. Akiba, H. Usui, M. Ochi, K. Kuroki, A. Miyake, M. Tokunaga, Y. Uwatoko, *et al.*, Physical review letters **122**, 226601 (2019).
- [4] C. Chu, T. Smith, and W. Gardner, Physical Review B **1**, 214 (1970).
- [5] M. Norman, J. Lin, and A. Millis, Physical Review B **81**, 180513 (2010).
- [6] K. Sandeman, G. Lonzarich, and A. Schofield, Physical review letters **90**, 167005 (2003).
- [7] C. L. Watlington, J. Cook Jr, and M. Skove, Physical Review B **15**, 1370 (1977).
- [8] Y. Yamaji, T. Misawa, and M. Imada, Journal of the Physical Society of Japan **76**, 063702 (2007).
- [9] E. Yelland, J. Barraclough, W. Wang, K. Kamenev, and A. Huxley, Nature physics **7**, 890 (2011).
- [10] C. Liu, T. Kondo, R. M. Fernandes, A. D. Palczewski, E. D. Mun, N. Ni, A. N. Thaler, A. Bostwick, E. Rotenberg, J. Schmalian, *et al.*, Nature Physics **6**, 419 (2010).
- [11] D. Xiao, M.-C. Chang, and Q. Niu, Reviews of modern physics **82**, 1959 (2010).
- [12] M. Z. Hasan and C. L. Kane, Rev. Mod. Phys. **82**, 3045 (2010).
- [13] X.-L. Qi and S.-C. Zhang, Rev. Mod. Phys. **83**, 1057 (2011).
- [14] N. P. Armitage, E. J. Mele, and A. Vishwanath, Rev. Mod. Phys. **90**, 015001 (2018).
- [15] N. Nagaosa, J. Sinova, S. Onoda, A. H. MacDonald, and N. P. Ong, Rev. Mod. Phys. **82**, 1539 (2010).
- [16] X. Wan, A. M. Turner, A. Vishwanath, and S. Y. Savrasov, Phys. Rev. B **83**, 205101 (2011).
- [17] S. Murakami, New Journal of Physics **9**, 356 (2007).
- [18] D. Son and B. Spivak, Physical Review B **88**, 104412 (2013).
- [19] I. Sodemann and L. Fu, Phys. Rev. Lett. **115**, 216806 (2015).
- [20] Q. Ma, S.-Y. Xu, H. Shen, D. MacNeill, V. Fatemi, T.-R. Chang, A. M. M. Valdivia, S. Wu, Z. Du, C.-H. Hsu, *et al.*, Nature **565**, 337 (2019).
- [21] Z. Z. Du, C. M. Wang, H.-Z. Lu, and X. C. Xie, Phys. Rev. Lett. **121**, 266601 (2018).
- [22] Z. Du, C. Wang, S. Li, H.-Z. Lu, and X. Xie, Nature communications **10**, 1 (2019).
- [23] M.-C. Chang and Q. Niu, Physical Review B **53**, 7010 (1996).
- [24] A. Knoll, C. Timm, and T. Meng, Physical Review B **101**, 201402 (2020).
- [25] G. Volovik, Low Temperature Physics **43**, 47 (2017).
- [26] Y. Zhang, C. Wang, L. Yu, G. Liu, A. Liang, J. Huang, S. Nie, X. Sun, Y. Zhang, B. Shen, *et al.*, Nature Communications **8**, 1 (2017).
- [27] G. E. Volovik, Physics-USpekhi **61**, 89 (2018).
- [28] H. Yang, L. Yang, Z. Liu, Y. Sun, C. Chen, H. Peng, M. Schmidt, D. Prabhakaran, B. A. Bernevig, C. Felser, *et al.*, Nature communications **10**, 1 (2019).
- [29] S. Ekahana, Y. Li, Y. Sun, H. Namiki, H. Yang, J. Jiang, L. Yang, W. Shi, C. Zhang, D. Pei, *et al.*, Physical Review B **102**, 085126 (2020).
- [30] Y. Wu, N. H. Jo, M. Ochi, L. Huang, D. Mou, S. L. Budjko, P. C. Canfield, N. Trivedi, R. Arita, and A. Kaminski, Physical Review Letters **115**, 166602 (2015).
- [31] A. A. Burkov, M. D. Hook, and L. Balents, Phys. Rev. B **84**, 235126 (2011).
- [32] Y. Kim, B. J. Wieder, C. L. Kane, and A. M. Rappe, Phys. Rev. Lett. **115**, 036806 (2015).
- [33] R. Yu, H. Weng, Z. Fang, X. Dai, and X. Hu, Phys. Rev. Lett. **115**, 036807 (2015).
- [34] T. T. Heikkilä, N. B. Kopnin, and G. E. Volovik, JETP Letters **94**, 233 (2011).
- [35] H. Weng, Y. Liang, Q. Xu, R. Yu, Z. Fang, X. Dai, and Y. Kawazoe, Phys. Rev. B **92**, 045108 (2015).
- [36] C. Fang, Y. Chen, H.-Y. Kee, and L. Fu, Phys. Rev. B **92**, 081201 (2015).
- [37] Y.-H. Chan, C.-K. Chiu, M. Y. Chou, and A. P. Schnyder, Phys. Rev. B **93**, 205132 (2016).
- [38] J. Zhao, R. Yu, H. Weng, and Z. Fang, Phys. Rev. B **94**, 195104 (2016).
- [39] T. Bzdusek, Q. Wu, A. Rüegg, M. Sigrist, and A. A. Soluyanov, Nature **538**, 75 (2016), letter.
- [40] W. Chen, H.-Z. Lu, and J.-M. Hou, Phys. Rev. B **96**, 041102 (2017).
- [41] Z. Yan, R. Bi, H. Shen, L. Lu, S.-C. Zhang, and Z. Wang, Phys. Rev. B **96**, 041103 (2017).
- [42] M. Ezawa, Phys. Rev. B **96**, 041202 (2017).
- [43] G. Bian, T.-R. Chang, R. Sankar, S.-Y. Xu, H. Zheng, T. Neupert, C.-K. Chiu, S.-M. Huang, G. Chang, I. Belopolski, *et al.*, Nature communications **7**, 1 (2016).
- [44] L. M. Schoop, M. N. Ali, C. Straßer, A. Topp, A. Varykhalov, D. Marchenko, V. Duppel, S. S. Parkin, B. V. Lotsch, and C. R. Ast, Nature communications **7**, 1 (2016).
- [45] M. Neupane, I. Belopolski, M. M. Hosen, D. S. Sanchez, R. Sankar, M. Szlowska, S.-Y. Xu, K. Dimitri, N. Dhakal, P. Maldonado, *et al.*, Physical Review B **93**, 201104 (2016).
- [46] A. Topp, J. M. Lippmann, A. Varykhalov, V. Duppel, B. V. Lotsch, C. R. Ast, and L. M. Schoop, New Journal of Physics **18**, 125014 (2016).
- [47] D. Takane, Z. Wang, S. Souma, K. Nakayama, C. Trang, T. Sato, T. Takahashi, and Y. Ando, Physical Review B **94**, 121108 (2016).
- [48] J. Hu, Z. Tang, J. Liu, X. Liu, Y. Zhu, D. Graf, K. Myhro, S. Tran, C. N. Lau, J. Wei, *et al.*, Physical review letters **117**, 016602 (2016).
- [49] J. Hu, Y. Zhu, D. Graf, Z. Tang, J. Liu, and Z. Mao, Physical Review B **95**, 205134 (2017).
- [50] N. Kumar, K. Manna, Y. Qi, S.-C. Wu, L. Wang, B. Yan, C. Felser, and C. Shekhar, Physical Review B **95**, 121109 (2017).



- [51] H. Pan, B. Tong, J. Yu, J. Wang, D. Fu, S. Zhang, B. Wu, X. Wan, C. Zhang, X. Wang, *et al.*, *Scientific reports* **8**, 1 (2018).
- [52] C. Li, C. Wang, B. Wan, X. Wan, H.-Z. Lu, and X. Xie, *Physical review letters* **120**, 146602 (2018).
- [53] J. Zhang, M. Gao, J. Zhang, X. Wang, X. Zhang, M. Zhang, W. Niu, R. Zhang, and Y. Xu, *Frontiers of Physics* **13**, 137201 (2018).
- [54] S. Li, Z. Guo, D. Fu, X.-C. Pan, J. Wang, K. Ran, S. Bao, Z. Ma, Z. Cai, R. Wang, *et al.*, *Science bulletin* **63**, 535 (2018).
- [55] Q. Chen, Z. Lou, S. Zhang, B. Xu, Y. Zhou, H. Chen, S. Chen, J. Du, H. Wang, J. Yang, *et al.*, *Physical Review B* **102**, 165133 (2020).
- [56] L. An, X. Zhu, W. Gao, M. Wu, W. Ning, and M. Tian, *Physical Review B* **99**, 045143 (2019).
- [57] T. Zhou, M. Tong, X. Xie, Y. Yu, X. Zhu, Z.-Y. Wang, and T. Jiang, *The Journal of Physical Chemistry Letters* **11**, 6475 (2020).
- [58] W. Chen, K. Luo, L. Li, and O. Zilberberg, *Phys. Rev. Lett.* **121**, 166802 (2018).
- [59] W. Chen, H.-Z. Lu, and O. Zilberberg, *Phys. Rev. Lett.* **122**, 196603 (2019).
- [60] W. Luo, W. Chen, and D. Y. Xing, *Sci. China Phys. Mech. Astron.* **64**, 267262 (2021).
- [61] X. Zhang, B. Fu, L. Jin, X. Dai, G. Liu, and Y. Yao, *The Journal of Physical Chemistry C* **123**, 25871 (2019).
- [62] W. Chen and J. L. Lado, *Phys. Rev. Lett.* **122**, 016803 (2019).
- [63] X. Dai, Z. Du, and H.-Z. Lu, *Physical review letters* **119**, 166601 (2017).
- [64] G. Sundaram and Q. Niu, *Physical Review B* **59**, 14915 (1999).
- [65] D. Xiao, J. Shi, and Q. Niu, *Physical review letters* **95**, 137204 (2005).
- [66] J. Bannies, E. Razzoli, M. Michiardi, H.-H. Kung, I. Elfmov, M. Yao, A. Fedorov, J. Fink, C. Jozwiak, A. Bostwick, *et al.*, *Physical Review B* **103**, 155144 (2021).
- [67] L. Guo, T.-W. Chen, C. Chen, L. Chen, Y. Zhang, G.-Y. Gao, J. Yang, X.-G. Li, W.-Y. Zhao, S. Dong, *et al.*, *ACS Applied Electronic Materials* **1**, 869 (2019).
- [68] S. Chen, Z. Lou, Y. Zhou, Q. Chen, B. Xu, C. Wu, J. Du, J. Yang, H. Wang, and M. Fang, *Chinese Physics Letters* **38**, 017202 (2021).
- [69] A. Laha, P. Rambabu, V. Kanchana, L. Petit, Z. Szotek, and Z. Hossain, *Physical Review B* **102**, 235135 (2020).
- [70] S. Sasmal, R. Mondal, R. Kulkarni, A. Thamizhavel, and B. Singh, *Journal of Physics: Condensed Matter* **32**, 335701 (2020).
- [71] S. Li, Z. Guo, D. Fu, X.-C. Pan, J. Wang, K. Ran, S. Bao, Z. Ma, Z. Cai, R. Wang, *et al.*, *Science bulletin* **63**, 535 (2018).